Solid State Sciences 11 (2009) 507–512

Contents lists available at ScienceDirect

Solid State Sciences

journal homepage: www.elsevier.com/locate/ssscie

Crystallographic and physical properties of $RE_{2-x}Ni_{21}B_6$ (RE = Er, Yb and Lu)

I. Veremchuk [a,b], R. Gumeniuk [a,*], Yu. Prots [a], W. Schnelle [a], U. Burkhardt [a], H. Rosner [a], Yu. Kuz'ma [b], A. Leithe-Jasper [a]

[a] Max-Planck-Institut für Chemische Physik fester Stoffe, Nöthnitzer Str. 40, 01187 Dresden, Germany
[b] Department of Analytical Chemistry, Ivan Franko National University of Lviv, Kyrylo and Mefodiy Street 6, 79005 Lviv, Ukraine

ARTICLE INFO

Article history:
Received 21 July 2008
Received in revised form 4 September 2008
Accepted 9 September 2008
Available online 30 September 2008

PACS:
06.60.Ei
61.05.cm
61.66.Dk
72.15.Eb
75.20.En

Keywords:
Crystal structure
Borides
Magnetic susceptibility
Electrical conductivity

ABSTRACT

Crystallographic and physical properties of cubic $Er_{2-x}Ni_{21}B_6$, $Yb_{2-x}Ni_{21}B_6$ and $Lu_{2-x}Ni_{21}B_6$ have been studied. Their crystal structures have been established from single-crystal and powder X-ray diffraction data (space group $Fm\bar{3}m$, $Cr_{23}C_6$ type of structure): $Er_{2-x}Ni_{21}B_6$, $a = 10.6520(2)$ Å, $R_F = 0.041$, $R_W = 0.044$ (for $x = 0.18$); $Yb_{2-x}Ni_{21}B_6$, $a = 10.6412(2)$ Å, $R_F = 0.021$, $R_W = 0.022$ (for $x = 0.14$); $a = 10.6243(2)$ Å, $R_F = 0.023$, $R_W = 0.025$ (for $x = 0.30$); $Lu_{2-x}Ni_{21}B_6$, $a = 10.6269(2)$ Å, $R_F = 0.023$, $R_W = 0.023$ (for $x = 0.35$). Small homogeneity ranges extend from $x = 0.1$–0.9 for $Er_{2-x}Ni_{21}B_6$ and from $x = 0.1$–0.3 for $Yb_{2-x}Ni_{21}B_6$. No homogeneity range was found for $Lu_{2-x}Ni_{21}B_6$ ($x = 0.35$). Magnetization measurements for $Yb_{2-x}Ni_{21}B_6$ and $Er_{2-x}Ni_{21}B_6$ reveal the $4f^{13}$ (Yb^{3+}) and $4f^{11}$ (Er^{3+}) electronic state and no magnetic ordering above 1.8 K. $RE_{2-x}Ni_{21}B_6$ compounds show metallic behavior in electrical conductivity.

1. Introduction

The class of "τ-boride" intermetallic compounds which adopt the cubic $Cr_{23}C_6$ type of structure (space group $Fm\bar{3}m$) [1], has about 85 representatives [2]. Rare-earth metal (RE) containing ternary borides with overall composition $RE_2Ni_{21}B_6$ (RE = Ho, Er, Tm, Yb, Lu) are known to exist. Atomic coordinates and displacement parameters were refined for $Lu_2Ni_{21}B_6$ [3] and $Ho_2Ni_{21}B_6$ [4] from powder x-ray diffraction (XRD). In the case of $Lu_2Ni_{21}B_6$ and $Ho_2Ni_{21}B_6$ compounds, the distances between the RE (occupying the 8*c* position) and Ni atoms (in 32*f*) are significantly smaller than the sum of atomic radii of the elements (shorter by about 13% for Ho and 17% for Lu). For many other borides of this family only lattice parameters have been reported so far [3]. The absence of detailed crystallographic data and metallographic investigations does not allow a deeper analysis of interatomic distances which would be necessary to understand structural features of these metal-rich borides.

During the systematic study of the Er–Ni–B and Yb–Ni–B ternary systems the $Er_2Ni_{21}B_6$ and $Yb_2Ni_{21}B_6$ borides were found [5,6]. Systematic variations of the lattice parameter have been observed in multiphase samples, which may indicate a possible homogeneity range. These preliminary results prompted us to perform a detailed investigation of the crystal structures of $Er_{2-x}Ni_{21}B_6$, $Yb_{2-x}Ni_{21}B_6$ and $Lu_{2-x}Ni_{21}B_6$.

2. Experimental

Samples (for compositions see Table 1) were prepared from filings of the corresponding rare-earth elements (Ames, 99.95 wt.%), Ni powder (100 mesh Chempur, 99.95 wt.%) or foil (Alfa Aesar, 99.99 wt.%) and crystalline B powder (<100 μm, Chempur 99.995 wt.%).

Corresponding rare-earth metals, nickel and boron were mixed and pressed into pellets (8 mm diameter). The samples were then arc-melted and remelted several times (weight loss 1–3%). All these manipulations were performed inside an argon-filled glove box ($p(O_2/H_2O) \leq 0.1$ ppm). For homogenization annealing each Yb- and Er-containing sample was put inside an Al_2O_3 crucible and sealed in a Ta tube. The tubes were enclosed in quartz ampoules and kept at 1100 °C for 4 days followed by 14 days at 800 °C and finally quenched in cold water. Samples containing Lu were arc-melted and then heat-treated in Ta tubes at 920 °C for 7 days. The

* Corresponding author. Tel.: +49 (0)351 46464275; fax: +49 (0)351 46464002.
E-mail address: gumeniuk@cpfs.mpg.de (R. Gumeniuk).

1293-2558/$ – see front matter © 2008 Elsevier Masson SAS. All rights reserved.
doi:10.1016/j.solidstatesciences.2008.09.004

Table 1
Composition and lattice parameters of $RE_{2-x}Ni_{21}B_6$ (RE = Er, Yb, Lu).

Nominal composition	Phases observed	Composition of the $RE_{2-x}Ni_{21}B_6$ phases (WDXS analysis)	Lattice parameter for $RE_{2-x}Ni_{21}B_6$
$Er_2Ni_{21}B_6$[a]	$Er_{2-x}Ni_{21}B_6 + ErNi_4B$	$Er_{1.77(6)}Ni_{20.5(1)}B_{6.7(2)}$	10.6520(2)
$Er_{1.7}Ni_{21}B_6$	$Er_{2-x}Ni_{21}B_6$	$Er_{1.63(9)}Ni_{20.9(1)}B_{6.5(2)}$	10.6334(2)
$Er_{1.5}Ni_{21}B_6$	$Er_{2-x}Ni_{21}B_6$	$Er_{1.45(9)}Ni_{20.9(1)}B_{6.6(2)}$	10.6240(3)
$Er_{1.0}Ni_{21}B_6$	$Er_{2-x}Ni_{21}B_6 + Ni_3B$	$Er_{0.96(9)}Ni_{21.5(1)}B_{6.6(1)}$	10.6170(2)
$Yb_2Ni_{21}B_6$[a]	$Yb_{2-x}Ni_{21}B_6 + YbNi_4B$	$Yb_{1.86(3)}Ni_{20.97(8)}B_{6.2(1)}$	10.6412(2)
$Yb_{1.7}Ni_{21}B_6$[a]	$Yb_{2-x}Ni_{21}B_6$	$Yb_{1.71(9)}Ni_{20.74(9)}B_{6.6(1)}$	10.6243(2)
$Yb_{1.5}Ni_{21}B_6$	$Yb_{2-x}Ni_{21}B_6 + Ni_3B$	$Yb_{1.68(3)}Ni_{20.76(7)}B_{6.5(1)}$	10.6229(2)
$Yb_{1.0}Ni_{21}B_6$	$Yb_{2-x}Ni_{21}B_6 + Ni_3B$	$Yb_{1.51(9)}Ni_{21.11(9)}B_{6.4(1)}$	10.6228(3)
$Lu_{1.5}Ni_{21}B_6$	$Lu_{2-x}Ni_{21}B_6 + Lu_2Ni_{17}$	–	10.6256(2)
$Lu_2Ni_{21}B_6$[a]	$Lu_{2-x}Ni_{21}B_6 + Lu_2Ni_{17}$	$Lu_{1.57(6)}Ni_{21.0(1)}B_{6.4(1)}$	10.6269(4)

[a] Samples from which single crystals were extracted.

resulting samples contained numerous irregular shaped crystals with metallic luster. They are stable in air for a long time.

All samples were characterized by powder XRD performed on a HUBER G670 imaging plate Guinier camera equipped with a Ge monochromator and Cu Kα_1 radiation ($\lambda = 1.54056$ Å). Phase analysis was performed by using the WinXPOW program package [7]. The lattice parameters were refined by least-squares fitting of powder data with LaB_6 as internal standard ($a = 4.1569$ Å) by using the WinCSD software [8].

Irregularly shaped crystals of $RE_{2-x}Ni_{21}B_6$ (RE = Er, Yb and Lu) were isolated from annealed samples. Their quality was checked by Laue photographs. The single-crystal intensity data were collected on a Rigaku AFC7 diffractometer equipped with a Mercury CCD detector applying Mo $K\alpha$ radiation ($\lambda = 0.71073$ Å).

For metallographic examination, pieces of about 3 mm diameter were cut from the annealed samples. They were embedded in epoxy resin. Grinding was performed on abrasive papers (500 and 1000 grit silicon carbide) with alcohol-based lubricants. Polishing was done using slurries of 9 and 3 μm diamond powder in alcohol-based lubricants. The microstructures were examined optically (Zeiss Axioplan 2) and with a scanning electron microscope (Philips XL 30). The compositions of the observed phases were analyzed by energy dispersive x-ray spectroscopy (EDXS) (Philips XL 30) and wavelength dispersive x-ray spectroscopy (WDXS) (Cameca SX 100) using $ErNi_5$, Yb_2Ni_{17}, $LuSi_2$ and Ni_3B as standards. The intensities of the lines B $K\alpha$, Ni $L\alpha$, Er $L\alpha$, Yb $M\beta$ and Lu $L\alpha$ were determined at an excitation current of 100 nA at 15 keV. Results from WDXS analysis are in good agreement with compositions deduced from analysis of powder XRD data and compositions derived from single-crystal data refinement (see Table 1), moreover no contamination by oxygen and/or carbon was detected.

The magnetization of polycrystalline sample pieces was measured in a SQUID magnetometer (MPMS XL-7, Quantum Design) in external fields between 20 Oe and 70 kOe and temperatures between 1.8 K and 400 K. Electrical resistivity was determined on cuboid-shaped polycrystalline blocks, cut from the annealed samples, by a dc four-point method between 4 K and 320 K. The estimated inaccuracy in $\rho(T)$ due to the geometry factor is ±20%. The heat capacity measurements were performed with a relaxation-type calorimeter (PPMS, Quantum Design) in magnetic fields up to 90 kOe between 1.8 K and 320 K for the Yb and Lu and up to 100 K for the Er compound on the samples used for resistivity measurements.

3. Results and discussion

3.1. Homogeneity ranges

To study the homogeneity ranges Er, Yb and Lu containing samples with various RE content have been synthesized (Table 1). Lattice parameters slightly decrease with decreasing of RE content, indicating following homogeneity ranges: $0.1 \le x \le 0.9$ for $Er_{2-x}Ni_{21}B_6$ and $0.1 \le x \le 0.3$ for $Yb_{2-x}Ni_{21}B_6$ compounds. WDXS investigation clearly confirmed this finding (Table 1). Thus, different partial occupancy of the 8c crystallographic position (see below) by RE atoms in the crystal structure leads to the existence of homogeneity ranges (Tables 2 and 3). No significant change of lattice parameters was observed in the case of the Lu compound: $a = 10.6256(2)$ Å for a sample with nominal composition $Lu_{1.5}Ni_{21}B_6$, which is within 3 e.s.d. equal to the value for a sample with the nominal composition $Lu_2Ni_{21}B_6$. This fact as well as the multiphase composition of all synthesized Lu samples, allow us to conclude on the constant composition $Lu_{1.65(6)}Ni_{21}B_6$ which was obtained from single-crystal XRD (Table 2). Thus, we observe a decrease of the extent of the homogeneity ranges with decreasing atomic radius of the RE atoms.

Table 2
Crystallographic data of $RE_{2-x}Ni_{21}B_6$ (space group $Fm\bar{3}m$, $Z = 4$).

Empirical formula	$Er_{1.82(5)}Ni_{21}B_6$	$Yb_{1.70(3)}Ni_{21}B_6$	$Yb_{1.86(2)}Ni_{21}B_6$	$Lu_{1.65(6)}Ni_{21}B_6$
Lattice parameter (a, Å)[a]	10.6520(2)	10.6243(2)	10.6412(2)	10.6269(4)
Cell volume, Å^3	1208.63(7)	1199.23(7)	1205.0(2)	1200.1(1)
Number of refined parameters	14			
$2\theta_{(max)}$	62.80	67.00	66.15	67.39
Index ranges	$-15 \le h \le 15$, $-15 \le k \le 12$, $-15 \le l \le 13$	$-15 \le h \le 16$, $-15 \le k \le 13$, $-16 \le l \le 11$	$-15 \le h \le 15$, $-10 \le k \le 15$, $-15 \le l \le 11$	$-16 \le h \le 15$, $-15 \le k \le 15$, $-11 \le l \le 15$
Reflections collected	2273	3231	2496	2655
Unique reflections	131	154	149	153
R_{int}	0.053	0.033	0.033	0.054
Observed reflections (with $F_{hkl} > 4\sigma(F)$)	131	139	149	139
Extinction coefficient	0.00010(2)	0.00170(8)	0.00099(5)	0.0041(2)
R_F/R_w[b]	0.041/0.044	0.023/0.025	0.021/0.022	0.023/0.023

[a] Lattice parameters were refined from powder diffraction data.
[b] $R_F = \sum||F_o|-|F_c||/\sum|F_o|$; $R_W = (\sum w(F_o^2-F_c^2)^2/\sum w(F_o^2)^2)^{1/2}$.

Table 3
Coordinates, displacement parameters and occupancy factors (G) for $RE_{2-x}Ni_{21}B_6$.

Atom	Site	Coordinates			$Er_{1.82}Ni_{21}B_6$		$Yb_{1.70}Ni_{21}B_6$		$Yb_{1.86}Ni_{21}B_6$		$Lu_{1.65}Ni_{21}B_6$	
					G, x or y	B_{iso}	G, x or y	B_{iso}	G, x or y	B_{iso}	G, x or y	B_{iso}
RE	8*c*	1/4	1/4	1/4	0.907(4)	0.63(1)	0.850(4)	0.58(1)	0.930(3)	0.53(1)	0.826(8)	0.47(2)
Ni1	4*a*	0	0	0		0.39(5)		0.38(3)		0.46(3)		0.41(3)
Ni2	32*f*	*x*	*x*	*x*	0.3875(1)	0.69(2)	0.38671(9)	0.70(1)	0.38715(6)	0.59(1)	0.38672(8)	0.59(2)
Ni3	48*h*	0	*y*	*y*	0.1690(1)	0.51(3)	0.16914(7)	0.46(2)	0.16893(5)	0.46(2)	0.16950(7)	0.45(2)
B	24*e*	*x*	0	0	0.270(2)	0.9(3)	0.270(1)	0.5(2)	0.270(1)	0.8(2)	0.269(1)	0.6(2)

3.2. Crystal structures

Single crystals were mechanically extracted from samples with nominal compositions $Er_2Ni_{21}B_6$, $Yb_2Ni_{21}B_6$, $Yb_{1.7}Ni_{21}B_6$ and $Lu_2Ni_{21}B_6$. Crystallographic details are presented in Table 2, atomic coordinates, isotropic and anisotropic displacement parameters are listed in Tables 3 and 4. The crystal structure of $Er_{1.5}Ni_{21}B_6$ compound has been refined from powder XRD data using a full profile method. The observed and calculated profiles are shown in Fig. 1 ($R_I = 0.059$, $R_P = 0.077$). All $RE_{2-x}Ni_{21}B_6$ compounds crystallize with the $Cr_{23}C_6$ type of structure [9]. In these compounds B atoms are occupying the 24*e* position of C atoms, while in three crystallographic sites (4*a*, 32*f* and 48*h*) occupied by Cr atoms in the prototype Ni atoms are situated. In all cases a partial occupancy of the 8*c* position by *RE* atoms is observed, which is in good agreement with results of WDXS analysis (see Table 1). This is a new feature for the first time observed in $RE_2Ni_{21}B_6$ borides [2] which has not been reported up to now. The anisotropic elongation of the displacement ellipsoid of the Ni2 atoms, being part of the coordination sphere of the *RE* atoms, in the direction towards the central atom (Table 4) is related to the vacancies.

The unit cell of $Lu_{1.65}Ni_{21}B_6$ as well as the coordination polyhedra of all atoms are presented in Figs. 2 and 3. The structural peculiarities of the arrangement of columns formed by polyhedra of Ni atoms consisting of tetragonal antiprisms (filled by B atoms) separated by a cubo-octahedron and an empty cube, were already reported earlier [9,10], other structural features of compounds with the $Cr_{23}C_6$ type of structure and its group – subgroup relation to a cubic close packed arrangement of Ni and B atoms are discussed in detail in [11] and [12]. The volume of the empty cube in the structure of the $Lu_{1.65}Ni_{21}B_6$ compound is about 14 Å^3, while the volume of the tetragonal antiprism, filled by B atoms, is ≈16 Å^3. Boron atoms in the structures of binary and ternary borides crystallizing with $CuAl_2$ and $BaAl_4$ types have tetragonal antiprismatic coordination [10]. So, in the structure of $ErFe_2B_2$ ($BaAl_4$ type) [13] the volume of the tetragonal antiprism is ≈24.1 Å^3 and in the structure of Ni_2B ($CuAl_2$ type) [14] boron atoms are situated in antiprisms with a volume of ≈18.1 Å^3.

The *RE* atoms are coordinated by 4Ni2 and 12Ni3 which form a Friauf polyhedron. Similarly to the previous results reported for $Ho_2Ni_{21}B_6$ [4], the minimal *RE*–Ni2 distances in the compounds with Er, Yb and Lu (Table 5) are much shorter than the sum of the atomic radii of the elements ($r_{Er} = 1.757$ Å, $r_{Yb} = 1.940$ Å, $r_{Lu} = 1.734$ Å, $r_{Ni} = 1.246$ Å, $r_B = 0.88$ Å [15]). A reduction of these distances by 15.5% in $Er_{1.82}Ni_{21}B_6$ and $Lu_{1.65}Ni_{21}B_6$ and 21% in $Yb_{1.70}Ni_{21}B_6$ is observed (the nearest neighbors of *RE* atoms are 4Ni2 atoms forming a tetrahedron (Fig. 3)). The same observation is made in $Al_3Ni_{20}B_6$ ($\delta_{Al-Ni} = 2.411$, $r_{Al} = 1.431$ Å, reduction of 10%) [12] and in $In_2Ni_{21}B_6$ ($\delta_{In-Ni} = 2.493$, $r_{In} = 1.626$ Å with reduction of 13.3%) [11]. The contraction increases with increasing r_R (R = p-elements or *RE* in 8*c* position). In the case of $Cr_{23}C_6$ the smallest distance $\delta_{Cr-Cr} = 2.437$ Å within the [Cr4] tetrahedron centered by Cr atoms in the 8*c* position is reduced only by 2.4% ($r_{Cr} = 1.249$ Å).

Such a significant decrease of interatomic distances is usually not observed in intermetallic compounds but quite frequently occurs in the structures of ternary borides containing Ni: $Er_{0.917}Ni_{4.09}B$ with $\delta_{Er-Ni} = 2.619$ Å [16], $Ho_2Ni_{15}B_6$ with $\delta_{Ho-Ni} = 2.666$ Å [17]. Also Yb atoms are in close contact with the other four Yb in a similar configuration of *RE*–4*RE* found in the Laves phase $YbNi_2$ ($\delta_{Yb-Yb} = 3.072$ Å with shortening of 20.8%) [18]. From these findings it can be deduced that the short distances observed in the $RE_{2-x}Ni_{21}B_6$ structure must be considered as inherent feature of this transition-metal-rich structure.

Table 4
Anisotropic displacement parameters in the crystal structures of $RE_{2-x}Ni_{21}B_6$.

Atom	B_{11}	B_{22}	B_{33}	B_{12}	B_{13}	B_{23}
$Er_{1.82}Ni_{21}B_6$						
Er	0.63(3)	B_{11}	B_{11}	0	0	0
Ni1	0.39(8)	B_{11}	B_{11}	0	0	0
Ni2	0.69(3)	B_{11}	B_{11}	0.18(3)	B_{12}	B_{12}
Ni3	0.68(6)	0.43(3)	B_{22}	0	0	−0.00(4)
$Yb_{1.70}Ni_{21}B_6$						
Yb	0.58(2)	B_{11}	B_{11}	0	0	0
Ni1	0.38(5)	B_{11}	B_{11}	0	0	0
Ni2	0.70(2)	B_{11}	B_{11}	0.25(2)	B_{12}	B_{12}
Ni3	0.56(4)	0.41(2)	B_{22}	0	0	0.00(3)
$Yb_{1.86}Ni_{21}B_6$						
Yb	0.53(2)	B_{11}	B_{11}	0	0	0
Ni1	0.46(4)	B_{11}	B_{11}	0	0	0
Ni2	0.59(2)	B_{11}	B_{11}	0.12(2)	B_{12}	B_{12}
Ni3	0.51(3)	0.44(2)	B_{22}	0	0	−0.03(2)
$Lu_{1.65}Ni_{21}B_6$						
Lu	0.47(3)	B_{11}	B_{11}	0	0	0
Ni1	0.41(6)	B_{11}	B_{11}	0	0	0
Ni2	0.59(3)	B_{11}	B_{11}	0.15(3)	B_{12}	B_{12}
Ni3	0.50(4)	0.43(3)	B_{22}	0	0	0.00(3)

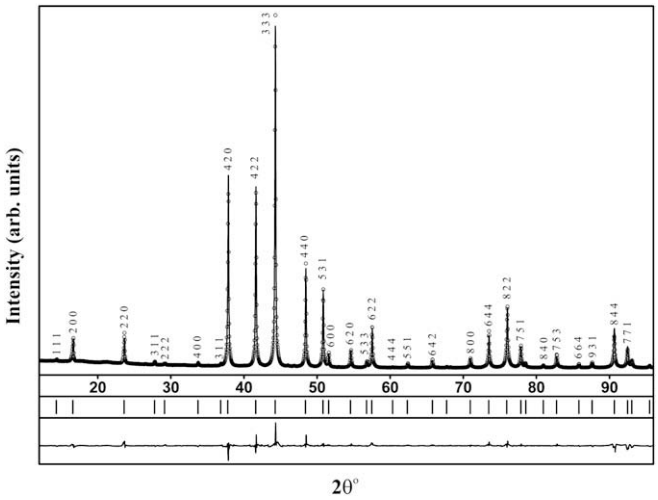

Fig. 1. Experimental (dots) and calculated (solid line) powder XRD patterns of $Er_{1.5}Ni_{21}B_6$ (Cu Kα_1 radiation) together with difference curve resulted from Rietveld refinement. Ticks correspond to calculated peaks positions.

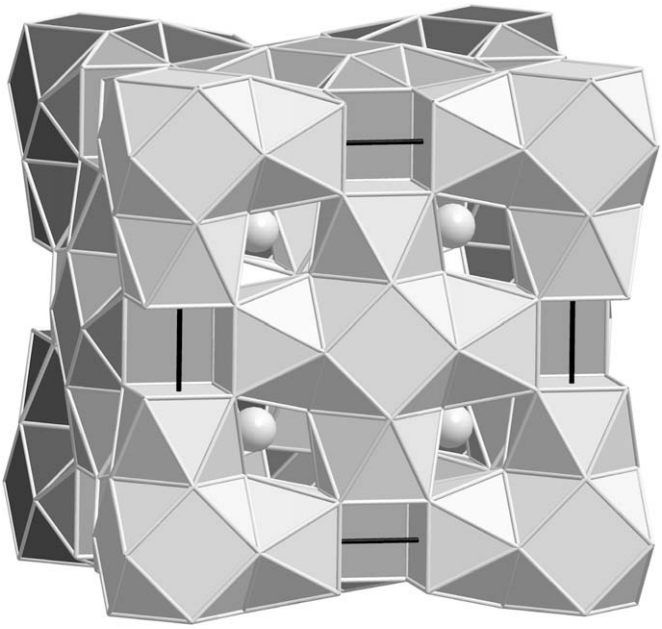

Fig. 2. 3D view of the stacking of the cubooctahedra and tetragonal antiprisms in the structure of $Lu_{1.65}Ni_{21}B_6$. White sphere: Lu atoms.

In the $RE_{2-x}Ni_{21}B_6$ compounds the Ni atoms possess coordination numbers (CN) of 12, 13 or 14 and isolated B atoms are situated in tetragonal antiprisms (CN = 8) formed by Ni atoms (Fig. 3 and Table 5). We do not observe shortening of more then 4% for δ_{Ni-Ni} or δ_{Ni-B} distances.

Compounds with the $Cr_{23}C_6$-type crystal structure containing RE are known in *RE*–Pd–{Si, Ge, P} and in the RE–Ni–B systems [19]. Moreover, they are reported in the R–R^1–{B, P} (R–*p*-element, R^1–*d*-element) systems [2]. The composition of the majority of these compounds is $R_2R^1{}_{21}B_6$, but for some of them deviate from this formula because some part of R^1-atoms are substituted by R-atoms (e.g.: $Al_3Ni_{20}B_6$, $Mn_3Co_{20}B_6$, $Mg_{3.5}Ni_{19.5}B_6$ [2]). Thus, the composition of these compounds may be described by $R_{2+n}R^1{}_{21-n}B_6$, which indicates a possibility of formation of homogeneity ranges. It has been observed that in the borides with the $Cr_{23}C_6$ ($R_{2+n}R'{}_{21-n}B_6$) structure type, the ratio r_R/r_R^1 usually is between 1.02 and 1.40 [10]. If R and R^1 components have similar atomic radii and are situated in neighboring groups of the periodic chart of elements, such borides may exhibit a homogeneity range by R/R' substitution. On the other hand, an increase of r_R/r_R^1 ratio and strong difference in electronic structure may lead to shrinking of the homogeneity ranges in ternary borides of this structure type. In case of {Er, Yb, Lu}$_{2-x}Ni_{21}B_6$ compounds we do not observe *RE*–Ni substitution.

3.3. Magnetic and electronic transport properties

The inverse magnetic susceptibility $H/M(T)$ of the $Yb_{1.7}Ni_{21}B_6$ sample (Fig. 4) is typical for the $^2F_{7/2}$ crystal electric field (CEF) ground state multiplet of the $4f^{13}$ configuration of Yb^{3+}. Usually, in intermetallic compounds of ytterbium, a Curie–Weiss fit for high temperatures gives values for the effective paramagnetic moment μ_{eff}. The determined μ_{eff} of 6.26 μ_B/f.u. (range of fit 150 K–400 K), is somewhat larger than expected (4.80 μ_B instead of 4.54 μ_B for free Yb^{3+} ions). The Weiss temperature Θ from the Curie–Weiss fit is negative ($\Theta_{high} = -32.9(8)$ K). In high-temperature fits of Yb^{3+} compounds the negative Θ usually does not indicate antiferromagnetic interactions but reflects the CEF splitting. For low-fields (20 Oe) a Curie–Weiss behavior is found down to 4.0 K. The Θ_{low} obtained from a Curie–Weiss fit between 4 K and 14 K is only

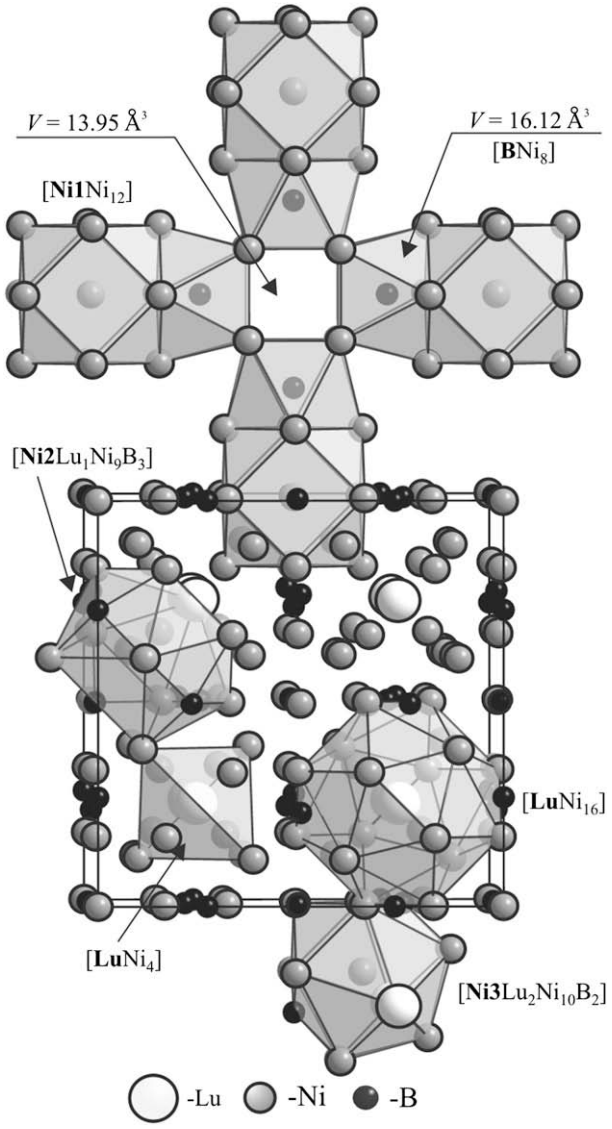

Fig. 3. The crystal structure of $Lu_{1.65}Ni_{21}B_6$: coordination polyhedra of atoms and arrangement of columns of tetragonal antiprisms separated by cubooctahedra and empty cubes.

Table 5
Interatomic distances (δ, Å) in the structures of $RE_{2-x}Ni_{21}B_6$.

Atoms		$Er_{1.82}Ni_{21}B_6$	$Yb_{1.70}Ni_{21}B_6$	$Yb_{1.86}Ni_{21}B_6$	$Lu_{1.65}Ni_{21}B_6$	CN
RE	−4Ni2	2.537(1)	2.516(1)	2.5277(7)	2.5165(9)	16
	−12Ni3	2.9295(5)	2.9207(3)	2.9267(2)	2.9192(3)	
Ni1	−12Ni3	2.545(1)	2.5413(7)	2.5422(6)	2.5474(7)	12
Ni2	−3B	2.11(1)	2.106(6)	2.108(7)	2.113(6)	13
	−3Ni2	2.397(2)	2.407(1)	2.4018(9)	2.408(1)	
	−1RE	2.537(1)	2.516(1)	2.5277(7)	2.5165(9)	
	−6Ni3	2.686(2)	2.673(1)	2.6815(8)	2.671(1)	
Ni3	−2B	2.10(1)	2.092(6)	2.094(6)	2.089(5)	14
	−1Ni3	2.442(2)	2.430(1)	2.4401(8)	2.420(1)	
	−1Ni1	2.545(1)	2.5413(7)	2.5422(6)	2.5474(7)	
	−4Ni3	2.545(1)	2.5413(7)	2.5422(6)	2.5474(7)	
	−4Ni2	2.686(2)	2.673(1)	2.6815(8)	2.671(1)	
	−2RE	2.9295(5)	2.9207(3)	2.9267(2)	2.9192(3)	
B	−4Ni3	2.10(1)	2.092(6)	2.094(6)	2.089(5)	8
	−4Ni2	2.11(1)	2.106(6)	2.108(7)	2.113(6)	

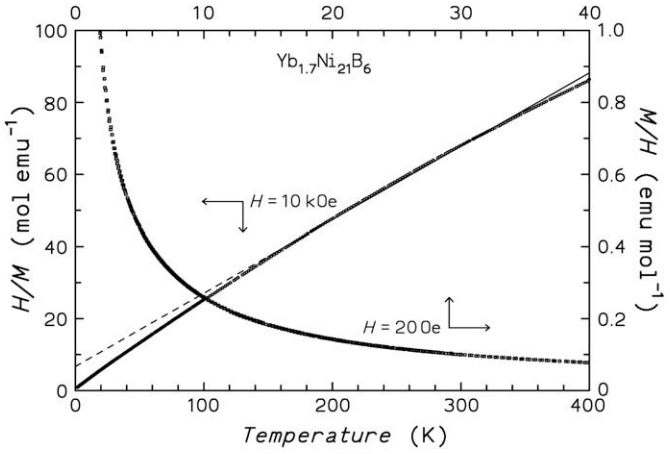

Fig. 4. Inverse magnetic susceptibility H/M of polycrystalline $Yb_{1.7}Ni_{21}B_6$ ($H_{ext} = 10$ kOe) and low-field low-temperature magnetic susceptibility M/H ($H_{ext} = 20$ Oe) vs. temperature. A Curie–Weiss fit to the high-field data (see text, solid line) and its extrapolation (dashed line) is shown.

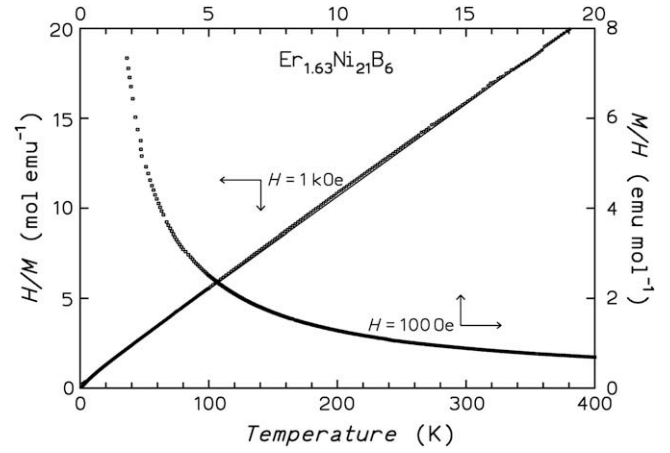

Fig. 5. Inverse magnetic susceptibility H/M of polycrystalline $Er_{1.63}Ni_{21}B_6$ ($H_{ext} = 1$ kOe) and M/H ($H_{ext} = 100$ Oe) vs. temperature. The solid line (almost coinciding with the data) is a Curie–Weiss fit.

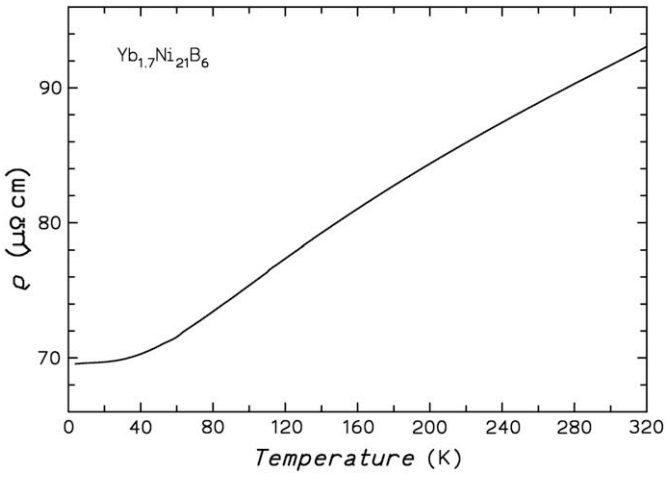

Fig. 6. Electrical resistivity $\rho(T)$ of polycrystalline $Yb_{1.7}Ni_{21}B_6$.

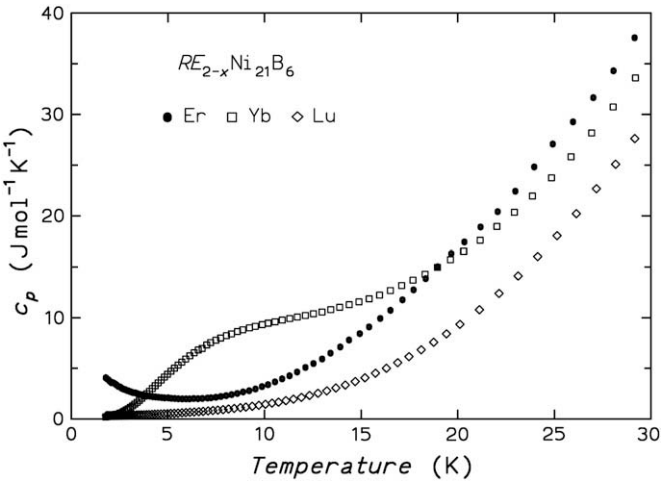

Fig. 7. Molar specific heat $c_p(T)$ vs. T for $Er_{1.63}Ni_{21}B_6$, $Yb_{1.7}Ni_{21}B_6$ and $Lu_{1.65}Ni_{21}B_6$.

−1.7 K, in agreement with the absence of magnetic order above 1.8 K.

The inverse magnetic susceptibility of the $Er_{1.63}Ni_{21}B_6$ sample (Fig. 5) is due to the $^4I_{15/2}$ CEF ground state of the $4f^{11}$ (Er^{3+}) species. μ_{eff} obtained from a Curie–Weiss fit (50 K < T < 400 K) is 9.50 μ_B/Er-atom ($\mu_{free} = 9.58\ \mu_B$), Θ is small ($\Theta_{high} = -6.02(7)$ K). Low-temperature Curie–Weiss fits for $H = 100$ Oe yield very small absolute values for $\Theta_{low} \approx -0.15$ K, consistent with the absence of magnetic ordering above 1.8 K. The Lu compound shows a small paramagnetic susceptibility.

The temperature dependence of the electrical resistivity $\rho(T)$ (Fig. 6) of the $Yb_{1.7}Ni_{21}B_6$ sample shows a large residual resistivity $\rho_0 = 70\ \mu\Omega$ cm while the temperature dependent part $\rho(300\text{ K}) - \rho_0 = 22\ \mu\Omega$ cm is much smaller. The large ρ_0 might be partially due to micro-cracks in the sample cut from this brittle material but more probably indicates a larger degree of intrinsic structural disorder. The Lu compound shows very similar characteristics ($\rho(300\text{ K}) = 95\ \mu\Omega$ cm, $\rho_0 = 60\ \mu\Omega$ cm), corroborating the above argumentation.

The molar specific heat $c_p(T)$ of these compounds is given in Fig. 7. The rare-earth ions in the Er and Yb compounds do not exhibit magnetic order; $c_p(T)$ is dominated by Schottky anomalies due to thermal population of CEF levels. The lattice contribution to $c_p(T)$ of the these compounds can be approximated by $c_p(T)$ of the Lu compound. After extraction of this contribution from the Lu compound data and subtraction of this lattice term from the Er and Yb compound data, the Schottky anomalies can be analyzed. In magnetic fields the CEF doublets (Yb^{3+} and Er^{3+} have Kramers half-integer J ground states) additionally split by the Zeeman effect. From fits it is possible to obtain the energies of all or of the lowest CEF levels (Yb: 0, 19.5(1.0) K, 47(5) K, 120(20) K; Er: 0, 60(4) K, 105(12) K, >400 K).

4. Conclusion

The crystal structures of $RE_{2-x}Ni_{21}B_6$ (RE = Er, Yb and Lu) were studied by means of single-crystal XRD for the first time (space group $Fm\bar{3}m$, $Cr_{23}C_6$ structure type). Compounds with Er and Yb have a homogeneity range ($Er_{1.1-1.9}Ni_{21}B_6$ and $Yb_{1.7-1.9}Ni_{21}B_6$) due to partial occupation of the 8*c* position. No mixed occupation by Ni and RE atoms is observed. It was shown, that $Er_{1.63}Ni_{21}B_6$ and $Yb_{1.7}Ni_{21}B_6$ do not order magnetically, the dependence of electrical resistivity upon temperature of Yb and Lu containing compounds is typically metallic, and the specific heats display Schottky anomalies in $Er_{1.63}Ni_{21}B_6$ and $Yb_{1.7}Ni_{21}B_6$ due to the crystal field splitting.

References

[1] A. Westgren, Nature 132 (1933) 480.
[2] (a) P. Villars, Pearson's Handbook, Crystallographic Data for Intermetallic Phases, vol. 1 (1997) Materials Park, OH 44073;
(b) Yu.B. Kuz'ma, N.F. Chaban, Binary and Ternary Systems Containing Boron, Handbook, Metallurgija, Moscow, 1990;
(c) H.H. Stadelmaier, in: B.C. Giessen (Ed.), Developments in the Structural Chemistry of Alloy Phases, Plenum Press, New York, London, 1969, pp. 141–181.
[3] N.F. Chaban, Yu.B. Kuz'ma, L.D. Kotovska, Dopov. Akad. Nauk URSR 42A (1980) 88–90.
[4] I.B. Gubych, Visnyk Lviv Univ., 31, 1991, pp. 5–8.
[5] N.F. Chaban, I. Veremchuk, Yu.B. Kuz'ma, J. Alloys Compd. 370 (2004) 129–132.
[6] I. Veremchuk, N. Chaban, Yu. Kuz'ma, J. Alloys Compd. 413 (2006) 127–132.
[7] STOE Powder Software, WinXPow (version 2.08), STOE and Cie GmbH, Darmstadt, 2003.
[8] (a) L.G. Akselrud, P.Y. Zavalii, Yu. Grin, V.K. Pecharsky, B. Baumgartner, E. Wölfel, Mater. Sci. Forum 133–136 (1993) 335–340;
(b) V.K. Pecharsky, P.Y. Zavalii, Fundamentals of Powder Diffraction and Structural Characterization of Materials, Springer, New York, 2005.
[9] A.L. Bowman, G.P. Arnold, E.K. Storms, N.G. Nereson, Acta Crystallogr. B28 (1972) 3102–3103.
[10] Yu. Kuz'ma, Crystal chemistry of borides, Vyshcha Shkola, Lvov. (1983).
[11] T. Adelsberger, M. Jansen, Z. Anorg. Allg. Chem. 625 (1999) 438–442.
[12] H. Hillebrecht, M. Ade, Angew. Chem., Int. Ed. 37 (7) (1998) 935–938.
[13] G.F. Stepanchikova, Yu.B. Kuz'ma, B.I. Chernjak, Dopov. Akad. Nauk URSR 40A (1978) 950–953.
[14] E.E. Havinga, H. Damsma, P. Hokkeling, J. Less Common Met. 27 (1972) 169–186.
[15] J. Emsley, The Elements, Clarendon Press, Oxford, 1995.
[16] Yu. Kuz'ma, V. Babizhetskyy, I. Veremchuk, N. Chaban, J. Solid State Chem. 177 (2004) 425–430.
[17] T. Gloviak, S.V. Orishchin, I.B. Gubych, N.F. Chaban, Yu.B. Kuz'ma, Sov. Phys. Crystallogr. 34 (1989) 602–604.
[18] K.H.J. Buschow, J. Less Common Met. 26 (1972) 329–333.
[19] Crystmet Version 4.4.0, The Metal Database, Toth Information System Inc., 1998–2008.